J Nanopart Res (2020) 22: 111
https://doi.org/10.1007/s11051-020-04846-2

RESEARCH PAPER

Crystal structure and electrical transport of nano-crystalline strontium-doped neodymium ortho-ferrites

I. A. Abdel-Latif

Received: 24 February 2020 / Accepted: 15 April 2020 / Published online: 8 May 2020

Abstract Strontium-doped neodymium orthoferrites belong to the perovskite type of materials of a wide range of interests and applications. This material has an orthorhombic perovskite crystal system of space group (Pbnm) no. 62. $Nd_{0.6}Sr_{0.4}FeO_3$ is synthesized using the co-precipitation method, and the resulting precipitated powder was fired at different temperatures to control the nano-crystalline size. The effect of the nano-crystalline size on the structure and the electrical properties were studied. The EDS spectra confirmed that the compound was formed according to the suggested calculations. SEM micrographs showed the homogeneity of the nano grain size in the compound. The nano-crystalline size of the prepared samples, fired at 705 °C and at 850 °C were 40 nm and 90 nm, respectively. $Nd_{0.6}Sr_{0.4}FeO_3$ showed a semiconducting behavior according to the exponential dependence of resistivity on temperature in the range from 350 K up to 473 K. The temperature independence of impedance is found at high frequencies starting from 0.5 MHz. The frequency dependence–activation energy is found in the temperature range from 350 K up to 473 K. The found decrease in AC resistivity with frequency increase for $Nd_{0.6}Sr_{0.4}FeO_3$ showed that the hopping mechanism occurred in the charge carrier transfer.

Keywords Perovskites · Nano-crystalline · Neodymium · Orthoferrites · Dielectric properties

This article is part of the topical collection: Nanotechnology in Arab Countries

Guest Editor: Sherif El-Eskandarany

I. A. Abdel-Latif
Physics Department, College of Science and Arts, Najran University, King Abdul Aziz Road,, P.O. 1988, Najran, Saudi Arabia

I. A. Abdel-Latif
Advanced Materials and Nano-Research Centre, Najran University, P.O. Box 1988, Najran 11001, Saudi Arabia

I. A. Abdel-Latif (✉)
Reactor Physics Department, Nuclear Research Center, Atomic Energy Authority, Abou Zaabal, P.O. 13759, Cairo, Egypt
e-mail: ihab_abdellatif@yahoo.co.uk

Introduction

The well-known rare earth orthoferrites, orthomanganites, orthocoblates, or orthonicklates are very rich materials because they have very interesting properties as well as a wide range of applications (Bashkirov Sh et al. 2005; Abdel-Latif et al. 2008; Hamad et al. 2017; Abdel-Latif et al. 2018a; Kurbakov et al. 2019). All of these interests were the motivation for more scientific curiosity to pursue research on these interesting topics in the hope of discovering more applications of these materials. Moreover, great efforts were carried out to find interpretations and propose new models that explain the unique and unusual phenomena found in these materials. These wide class of materials could be formed in different crystalline structures and showed crystalline phase transformations because of different annealing temperatures (Abdel-Latif et al. 2015; Kumar 2016). They are stable materials, and

they showed very interesting chemical properties such as chemical sensing, (Shuk et al. 1993; Abdel-Latif et al. 2018b; Shuk and Guth 1995) and photocatalytic properties (Abdel-Latif et al. 2019; Abdel-Latif et al. 2017; Kanhere 2014). Both magneto-electrical and magneto-caloric properties are found for these materials such as magnetoresistance (Bouziane et al. 2005; Petrov et al. 1999), magneto-caloric effect (Ahmed et al. 2019; Bettaibi et al. 2016); moreover, multiferroics properties that are clear in these types of materials (Lee et al. 2008; Ramesh and Spaldin 2007; LEE et al. 2005). All these properties have opened the door to apply them in magnetic devices (Abdel-Latif et al. 2016; Zhang et al. 2016; Tugova et al. 2017); magnetic cooling (Ayas 2017; Chandran et al. 2019; Cherif et al. 2014) and magnetic storage media (Kundu 2016; Kim et al. 2019; Pattnaik et al. 2019). They have different crystallographic crystal systems (cubic, orthorhombic, hexagonal, monoclinic, and rhombohedral crystal system) and this is the main reason for the various characteristics of these materials (Elghoul et al. 2018, Mahato Dev et al. 2016, Tokunaga et al. 2006). Rare earth ferrites are shaped with various crystallographic symmetries (Bashkirov Sh et al. 2003; Parfenov et al. 2003; Abdel-Latif 2011; Parfenov 2007; Yousif et al. 2011; Abdel-Latif 2016; Markovich et al. 2013; Iqbal et al. 2012). Type of the formed crystallographic symmetry depends on two main parameters: the temperature treatment and the ionic radius of the A-site element and doping divalent element or rare earth element (Abdel-Latif 2020). The orthorhombic distortion of the perovskite-like structure ABO_3 is one of the common structures these compounds have. The A sites in such materials are surrounded by quite distorted twelve oxygen atoms polyhedral while the B atoms are less distorted and they are surrounded by six oxygen atoms forming an octahedron. When an octahedron in these compounds is tilted, the occurring tilt causes tilting of the neighboring octahedra. The magnetoresistance that originated because of hole doping is shown in the orthorhombic the rare earth ferrite type (so called orthoferrites).

The dielectric loss factor measurements may help to understand different types of polarization mechanisms such as Maxwell–Wagner, ionic, dipole, and electronic (Saleh et al. 2020) as well as electric conduction. Grain boundaries formed during the annealing process play a fundamental role in the crystallization and the low surface area besides the oxidation state (Iqbal et al. 2017). The grain boundary contribution is noted and clear when the high resistivity of under-investigation materials at low frequency is measured (Naseem et al. 2018).

In the present work, $Nd_{0.6}Sr_{0.4}FeO_3$ is prepared by using the co-precipitation method and it is fired at various temperatures in order to get grains with different sizes. The effect of the nano-crystalline size on electrical and dielectric properties in $Nd_{0.6}Sr_{0.4}FeO_3$ is studied.

Experimental details

The strontium-doped neodymium orthoferrite compound under study was synthesized using the co-precipitation method. Highly pure chlorides (purity 99.9%, Sigma-Aldrich) were used: $FeCl_3{\cdot}4H_2O$, $NdCl_3{\cdot}6H_2O$, and $SrCl_2{\cdot}4H_2O$. These pure chlorides (16.68 g of $FeCl_3{\cdot}4H_2O$, 5.38 g of $NdCl_3{\cdot}6H_2O$, and 2.68 g mol of $SrCl_2{\cdot}4H_2O$) are dissolved in 100 mL distilled water to react with 5 g of NaOH. The mixed solution was kept stirred for 6 h at temperature of 85 °C, and we adjusted the pH to be 12. The precipitation process was started; the resulting precipitated powder needed separation, and so it was washed by distilled water many times, until NaCl was removed and only the formed strontium-doped neodymium orthoferrite remained. The separated powder is carefully milled to be pressed into the disc shape of 10-mm diameter. This disc is fired at the start of the annealing process at different temperatures. The firing temperatures in our case were 750 and 850 °C, in air for 12 h, and cooling was done at furnace temperature. The XRD patterns were measured using a PANalytical X'Pert Pro MPR diffractometer which produced a Cu radiation of 1.54 Å wavelength. The morphology of the compound was studied using a field emission scanning electron microscope (FE-SEM: JEOL JSM-7600F). The energy-dispersive EDS spectrum was used to examine the chemical purity of the formed $Nd_{0.6}Sr_{0.4}FeO_3$. Both the AC and DC resistivity temperature-dependent measurements were done in the temperature range from room temperature up to 473 K. The dielectric characteristics were collected as a function of temperature and frequency (LCR) meter (HP4284A). The DC resistivity measurements were carried out as a function of temperature using the two- and four-point probe technique (Scientific Equipment Service).

Results and discussions

The crystallization of rare earth ferrite, manganite, coblate, or niclate oxides occurred in a certain way as to take the perovskite-like structure (Bashkirov Sh et al. 2005; Kurbakov et al. 2019; Abdel-Latif et al. 2018b; Abdel-Latif et al. 2019). This type of perovskite-like structure can be found in different crystal systems where it takes the simple cubic form and transforms into another crystal structure phase, such as orthorhombic, hexagonal, monoclinic, or rhombohedral structure. This difference is attributed to the method of synthesis and the annealing process during preparation. The great diversity in crystallization in various forms leads to a wide scale of interests correlated to each structure form as well as the change in the crystal structure at low temperature. The EDS test of the strontium-doped neodymium orthoferrite compound under study showed that it is formed according to the calculated formula and all the constituent elements in the compound are formed with the right percentage.

XRD structure analysis

In the present work, XRD patterns of $Nd_{0.6}Sr_{0.4}FeO_3$ are measured at room temperature for as-prepared samples as well as samples fired at 750 °C and at 850 °C. These measurements were done using a Cu X-ray tube of wavelength 1.54 Å according to a step scan regime from angle $2\theta = 10°$ up to 90°. The XRD patterns were analyzed to check the forming of the designed orthorhombic phase structure. It is clear from Fig. 1a that the orthorhombic phase is formed after annealing at 750 °C and 850 °C temperatures. All the peaks in the XRD patterns are indexed, and it is clear that the orthorhombic crystal structure system of space group no. 62 (Pbnm) is satisfied.

The crystalline phase is not completely formed in the as-prepared sample, but because of the annealing process (at 750 °C and 850 °C), the crystalline phase is completely formed. The formation required in the crystal structure as a result of annealing is observed in the nanoscale. The experimental XRD patterns of the fired samples are fitted based on the Rietveld refinement method by using FullProf package software (Rodriguez-Carvajal 1993), and all the calculated lattice parameters from the refinements are listed in Table 1. The indexing of all the reflection peaks in the measured XRD patterns is done according to orthorhombic crystal system of space group Pbnm (no. 62). All generated hkl planes are shown in the CIF file as well as the Rietveld refinement parameters.

The resulting lattice constants of $Nd_{0.6}Sr_{0.4}FeO_3$ fired at 750 °C and 850 °C, which are listed in Table 1, are in good agreement with those previously reported (Dasgupta et al. 2002). There is slight change in the lattice constant, bond lengths, and angle between iron and oxygen atoms. This difference is attributed to the difference in the annealing temperature which may affect how oxygen atoms are occupying their positions and forming the octahedral side around the iron atoms. There are differences in the bond lengths and angle between iron and oxygen which are the two main parameters in electronic and magnetic transfer. On the other hand, the difference in crystalline size in both samples is clear because of the various annealing temperatures. The crystalline size could be deduced from the well-known Scherrer equation where the broadness of the peaks is analyzed and taking into consideration the instrumental broadening (Abdel-Latif 2011) to avoid a dramatical error:

$$\text{Cryst size } \delta = \frac{K\lambda}{B\sin\theta} \tag{1}$$

where the broadening in the peak (FWHM) is represented by B which is equal to the difference between that measured in the experimental XRD pattern for sample B_{obs}. and that measured for the standard sample B_{std}. The importance of this crystalline size is because it plays a principal role in the dependence of the physical and chemical properties.

Electron density $\rho(r)$ calculations as a result of the scattering of incident X-ray on the unit cell are done using a subprogram in FullProf software package. These calculations are based on Fourier method and fast Fourier transform (FFT). The following equation was applied for the density of electrons (DOE) based on FFT in the fitted XRD data, estimating the density of electrons (Abdel-Latif et al. 2016):

$$\rho(r) = \frac{1}{V}\sum_{H} F(H)\exp\{-2\pi i(H\cdot r)\} \tag{2}$$

It is clear that the electron density equation consists of the following parts: for the unit cell, there are the volume (V), the position vector inside the unit cell (r), and the reciprocal lattice vector (H) besides the coefficients of the complex Fourier $F(H)$. The density of

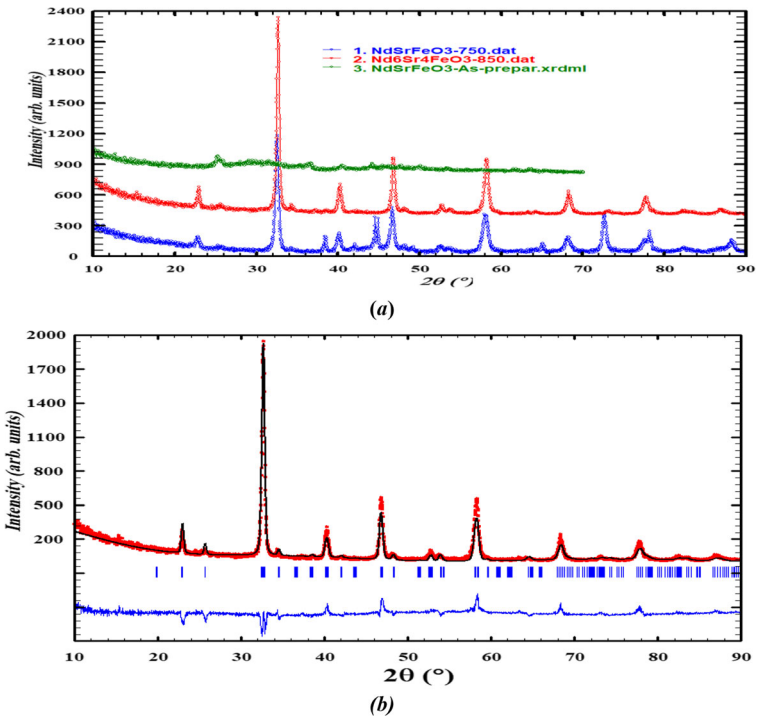

Fig. 1 XRD partners of **a** as-prepared samples as well as samples fired at 750 °C and at 850 °C at room temperature and of **b** $Nd_{0.6}Sr_{0.4}FeO_3$ fired at 850 °C with Rietveld analysis at room temperature

electrons has the same units of the complex Fourier $F(H)$ per volume (Abdel-Latif 2020). From the distribution of electrons inside the unit cell, it is clear that there are more electrons in the position of iron atoms in the case of annealing at 850 °C than in the case of annealing at 750 °C. This difference in the electron density will help us to understand the electric and magnetic properties dependent on the annealing temperature (Fig. 2).

Table 1 Lattice parameters, crystalline size, bond lengths, and angles between iron and oxygen in the $Nd_{0.6}Sr_{0.4}FeO_3$ samples fired at 750 °C and at 850 °C

$Nd_{0.6}Sr_{0.4}FeO_3$	750 °C	850 °C
a (Å)	5.483 (4)	5.4709 (8)
b (Å)	5.536 (4)	5.5158 (6)
c (Å)	7.748 (6)	7.7480 (12)
V (Å^3)	235.2 (3)	233.81 (6)
Cryst size (nm)	24	72
Fe-O_2 (Å)	1.957 (19)	2.02 (3)
Fe-O_2 (Å)	1.999 (19)	2.06 (3)
Fe-O_1 (Å)	1.9470 (15)	1.9469 (3)
Fe-O_2-Fe	160.0 (8)	145.1 (11)
Fe-O1-Fe	168.39 (19)	168.42 (4)

The representation of the unit cell based on the CIF file which resulted from Rietveld refinement is done using Diamond software, and it is shown in Fig. 3. It is clear that there is a slight difference in the atomic position in the unit cell which may effect its properties.

EDXS and SEM analysis

The elemental analysis based on EDXS spectra was done for $Nd_{0.6}Sr_{0.4}FeO_3$ as shown in Fig. 4. The used accelerating voltage for collecting spectrum was 15 keV. Analyzing the intensity under the peaks for all elements in the spectrum, one found that there is good agreement between the experimentally observed percentages of elements and the theoretically calculated. This good agreement showed that the obtained compound is formed in the proper way according to the proposed structure and all elements existed at the right percentage. The nano-crystalline size from the SEM micrographs of $Nd_{0.6}Sr_{0.4}FeO_3$ annealed at 750 °C and 850 °C is in good agreement with those calculated from XRD analysis in the range from 20 nm up to 100 nm. The average size is 40 nm for NSFO-750 °C and 90 nm for NSFO-850 °C.

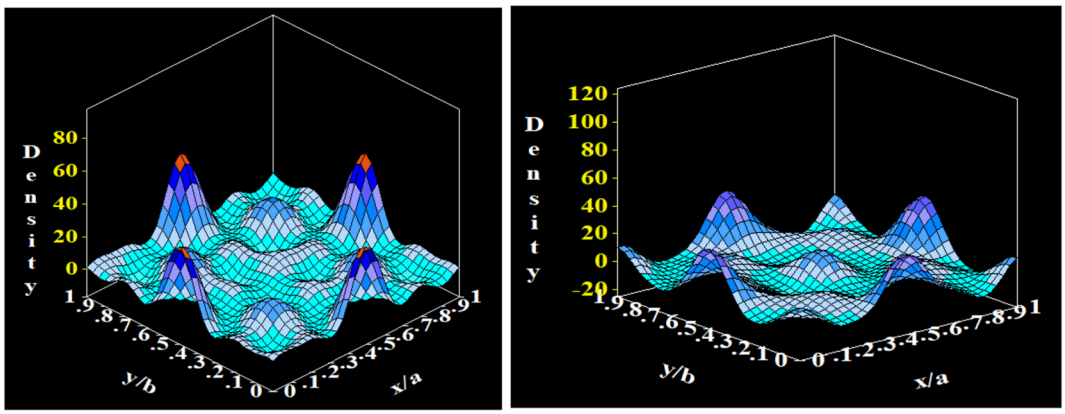

850°C 750°C

Fig. 2 Electron density map representation inside the unit cell of $Nd_{0.6}Sr_{0.4}FeO_3$ fired at 750 °C and 850 °C

Transport properties of $Nd_{0.6}Sr_{0.4}FeO_3$

To understand the electrical transport in the strontium-doped neodymium orthoferrite resistivity under investigation, measurements for temperature dependence were done. The variation in AC resistivity measurements as a function of temperature are shown in Figs. 5, 6, 7, and 8. The exponential relation between resistivity and temperature is found in the temperature range from 350 K up to 473 K to show the semiconducting properties of these materials under study (Parfenov 2007; Yousif et al. 2011).

The AC resistivity as a function of frequency and temperature was analyzed for $Nd_{0.6}Sr_{0.4}FeO_3$. The

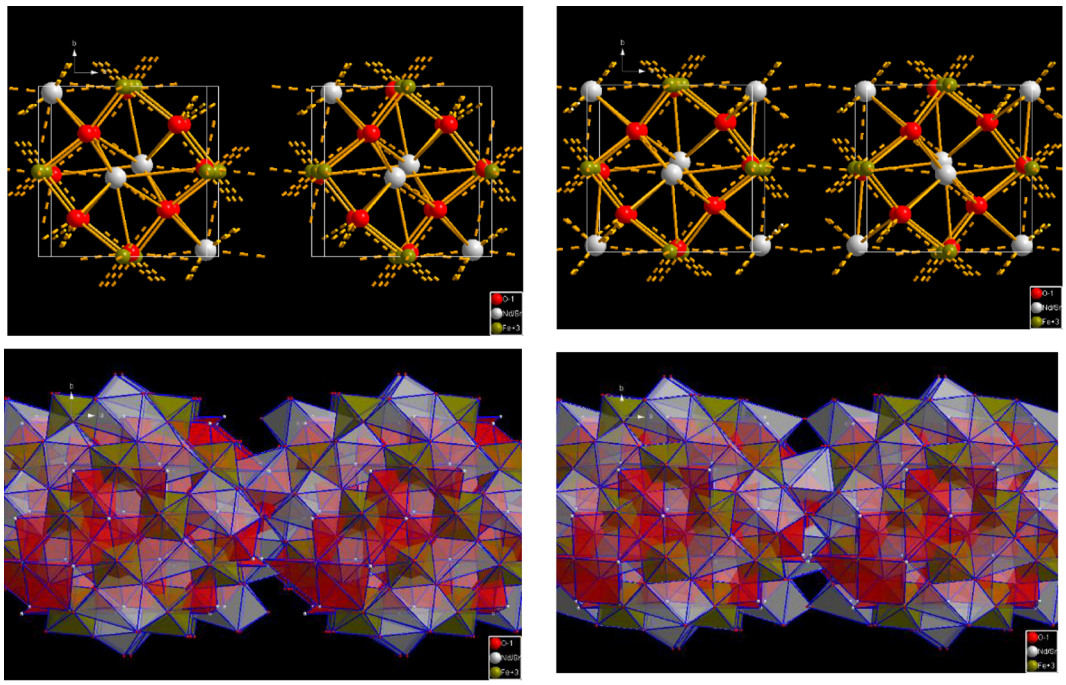

850°C 750°C

Fig. 3 Unit cell representation of $Nd_{0.6}Sr_{0.4}FeO_3$ fired at 750 and 850 °C

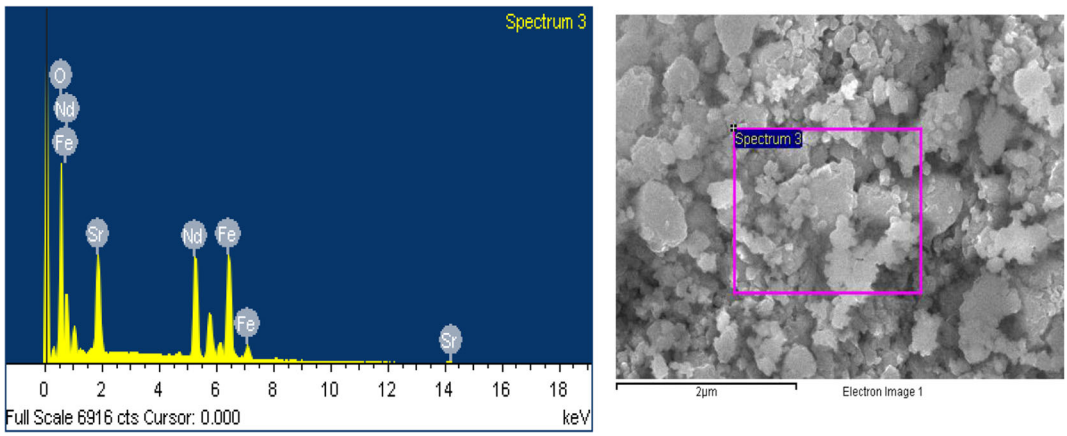

Fig. 4 EDS spectrum and SEM micrograph of $Nd_{0.6}Sr_{0.4}FeO_3$

decrease in AC resistivity in NSFO-750 °C as a result of the increase in frequency is clear as shown in Fig. 6. The present behavior enhances the hopping mechanism in NSFO-750 °C (Rajwali and Fang 2015). This type of AC conductivity–frequency dependency may be interpreted in terms of series resistance effect according to what was reported before. The strong correlation between AC resistivity of any materials and the hopping of weakly bound charge carriers is clear in the NSFO-750 °C under investigation and is similar to those reported in Ahmad et al. (2018).

The frequency dependence–activation energy is represented in Fig. 8. The obtained results confirm the semiconducting behavior of NSFO-750 °C in the temperature range from 350 K up to 473 K. The activation energy at low frequency is closed to each other and near the value of DC resistivity dependent on temperature (zero frequency case).

The relation between the complex impedance Z and microstructure of polycrystalline is strongly pronounced where the grain size is a very important parameter which may affect Z values. There are other parameters that may affect on complex impedance such as the temperature, frequency, and conductivity type. Knowing the conduction mechanism dependency on the complex impedance measurements helps us to understand the electronic transfer. In general, the electrical properties may be expressed in terms of two parameters: the real and imaginary parts of impendence (Dadami et al. 2017)

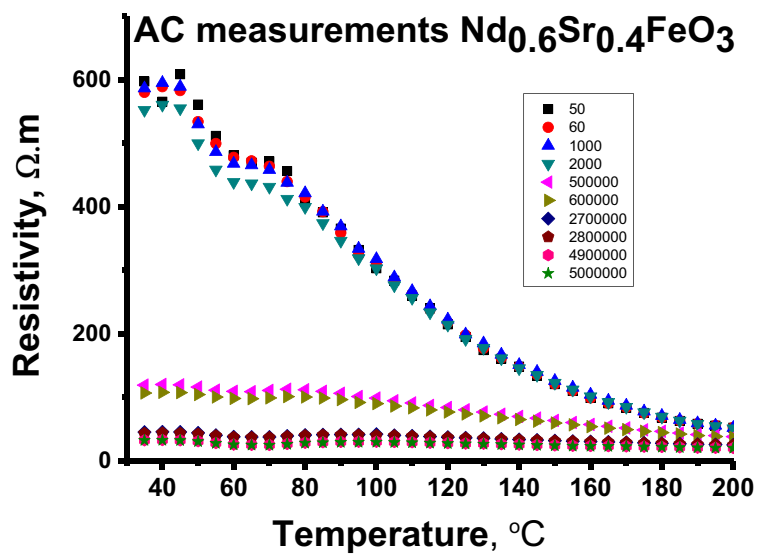

Fig. 5 AC resistivity variation as function of temperature for different frequencies

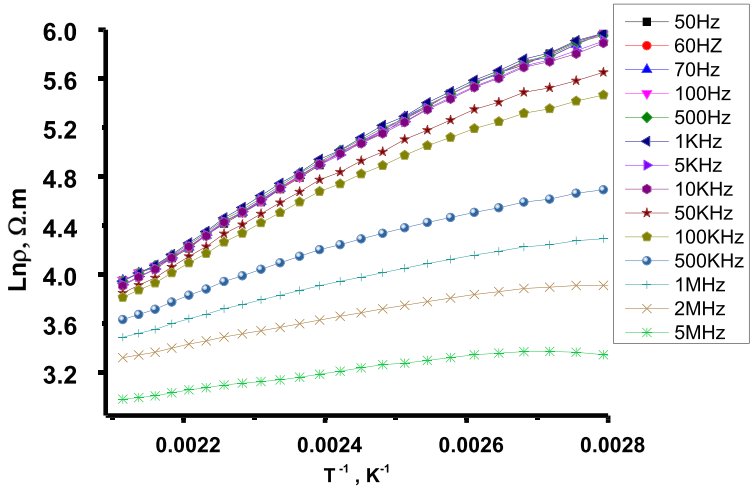

Fig. 6 The linear dependence of ln ρ_{ac} on inverse temperature for NSFO-750C at different frequencies

$$Z^* = Z' + jZ'' \tag{3}$$

where the real part is defined as $Z' = |Z| \cos\theta$ and $Z'' = |Z| \sin\theta$ is the imaginary part. Impedance–temperature dependence measurement at various frequencies of $Nd_{0.6}Sr_{0.4}FeO_3$ annealed at 750 °C (NSFO-750 °C) is shown in Fig. 5.

The high value of the impedance at low frequency is clear and followed by a sharp decrease when both temperature and frequencies increased. In other words, we can note the temperature independence of impedance which has been started from 0.5 MHz at high frequencies.

Electric conduction and different polarization mechanisms are parameters that depend on the dielectric loss factor (Komarov et al. 2005). Permittivity is a physical parameter that is used to find the dielectric properties. From the electromagnetic wave reflection at interfaces and the occurring attenuation of wave energy within materials, we can get permittivity and may be expressed as

$$\varepsilon^* = \varepsilon' + j\varepsilon'' \tag{4}$$

where ε' is the real permittivity and ε'' is the imaginary permittivity in the equation of permittivity (Saleh et al. 2020).

The ε' real and ε'' imaginary parts of the dielectric dependence on frequency can be written using the impedance data accordingly:

$$\varepsilon' = \frac{Z''}{2\pi f C_0 \left[(Z')^2 + (Z')^2 \right]}$$
$$\varepsilon'' = \frac{Z'}{2\pi f C_0 \left[(Z')^2 + (Z'')^2 \right]} \tag{5}$$

where Z' is the real impedance part and Z'' is the imaginary impedance part; C_o is the geometrical capacitance and f is the frequency.

Looking at variation in dielectric loss dependent on frequency at different temperatures shown in Fig. 9, one can see the high value of dielectric loss at very low frequencies then a sharp decrease in dielectric loss. This behavior is repeated, but the decrease is not so sharp like in room temperature. The sharp decrease in dielectric loss, with frequency increase, is less at high temperature measurements, 423 and 473 K, as clearly shown in Fig. 9, where the dielectric loss is independent on frequency at very high frequency (dielectric dispersion). This behavior can

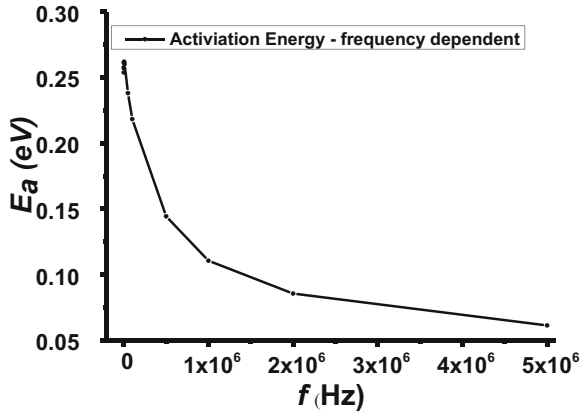

Fig. 7 Frequency dependence of activation energy E_a in NSFO-750C

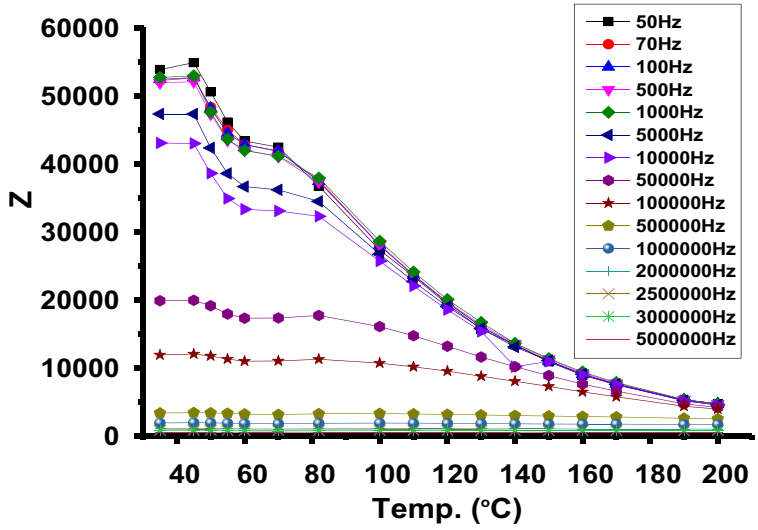

Fig. 8 The correlation between the impedance and temperature of NSFO-750C at different frequencies

be interpreted in terms of conducting grains generated in nano-structure in consistent with the Maxwell and Wagner's bilayer model and Koops phenomenological theory (Bhasin et al. 2018). Moreover, the dielectric loss tangent tan δ gives us information about the energy loss. It is the real permittivity divided by the imaginary dielectric permittivity equation:

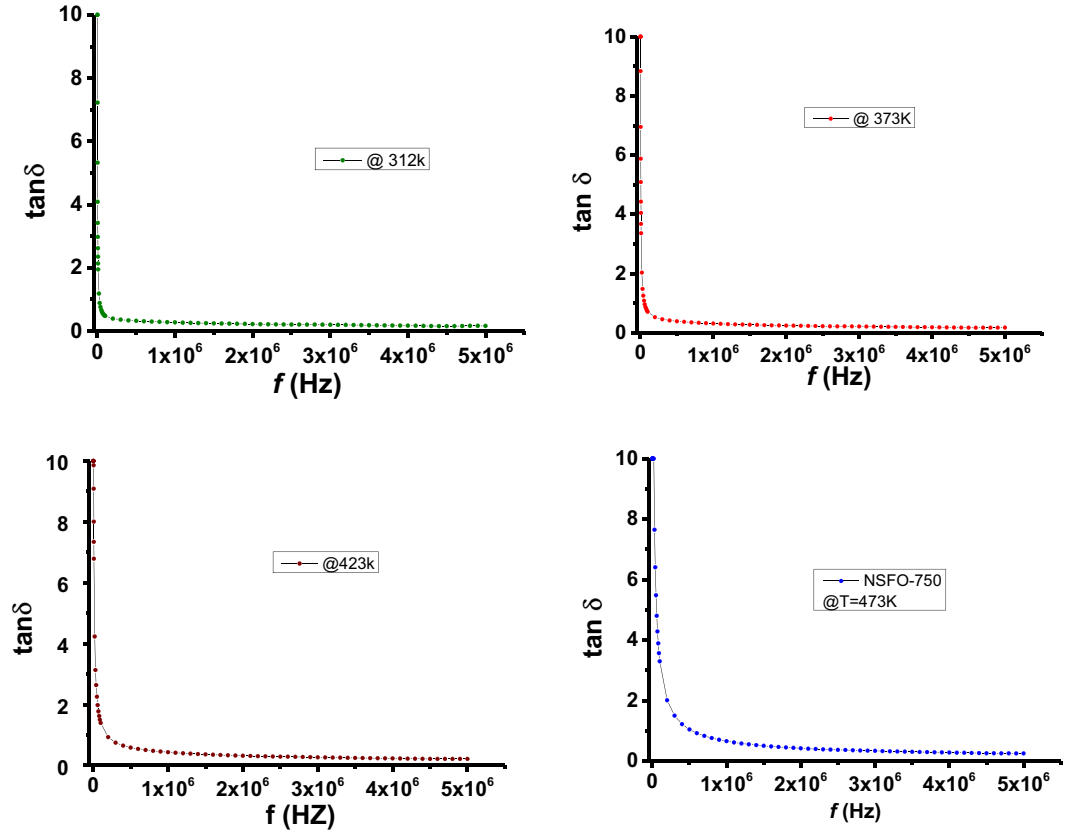

Fig. 9 Variation in dielectric loss dependent on frequency at different temperatures

$$D = \tan\delta = \frac{\varepsilon''}{\varepsilon'} \quad (6)$$

where δ is the phase difference between the applied field and the induced current in the material (Varshney et al. 2018). The observed decrease in tan δ, in our case, with frequency increase, is mainly based on two parameters: resistive loss and relaxation loss. In resistive loss, the mobility of charge has a great effect, but in relaxation loss, the dipole effect is more pronounced (Sharma et al. 2014).

Conclusions

- The orthorhombic crystal structure system of space group Pbnm is found.
- The obtained nano-crystalline sizes of the prepared $Nd_{0.6}Sr_{0.4}FeO_3$ samples, fired at 705 °C and at 850 °C, were 40 nm and 90 nm, respectively.
- The found decrease in AC resistivity with frequency increase gives the interpretation for the charge carriers transfer mechanism in $Nd_{0.6}Sr_{0.4}FeO_3$ as hopping mechanism.
- The temperature independence of impedance is found at high frequencies starting from 0.5 MHz.

Funding information The present research is supported by the Deanship of Scientific Research fund program in Najran University. The author was financially supported by NU/ESCI/16/062, given to him in the frame of the local scientific research program support.

Compliance with ethical standards

Conflict of interest The author declares that he has no conflict of interest.

References

Abdel-Latif IA, Hassen A, Zybill C, Abdel-Hafiez M, Allam S, El-Sherbini T (2008) The influence of tilt angle on the CMR in $Sm_{0.6}Sr_{0.4}MnO_3$. J Alloys Compd 452:245–248. https://doi.org/10.1016/j.jallcom.2007.07.022

Abdel-Latif IA, Ahmed AM, Mohamed HF, Saleh SA, Paixão JA, Ziq Kh A, Hamad M, Al-Nahari EG, Ghoza M, Allam S (2018a) Magnetocaloric effect, electric, and dielectric properties of $Nd_{0.6}Sr_{0.4}Mn_xCo_{1-x}O_3$ composites. J. Magnetism and Magnetic Materials 457:126–134. https://doi.org/10.1016/j.jmmm.2018.02.087

Abdel-Latif IA et al (2015) Synthesis of novel perovskite crystal structure phase of strontium doped rare earth manganites using sol gel method. J Magn Magn Mater 393:233–238. https://doi.org/10.1016/j.jmmm.2015.05.078

Abdel-Latif IA, Rahman MM, Khan SB (2018b) Neodymium cobalt oxide as a chemical sensor. Results in Physics 8: 578–583. https://doi.org/10.1016/j.rinp.2017.12.079

Abdel-Latif IA, Al-Hajji LA, Faisal M, Ismail AA (2019) Doping strontium into neodymium manganites nanocomposites for enhanced visible light driven photocatalysis. Sci Rep 9: 13932. https://doi.org/10.1038/s41598-019-50393-9

Abdel-Latif IA, Ismail AA, Faisal M, Ali AM, al-Salmi AE, al-Hajry A (2017) Impact of the annealing temperature on perovskite strontium doped neodymium manganites nanocomposites and their photocatalytic performances. J Taiwan Inst Chem Eng 75:174–182. https://doi.org/10.1016/j.jtice.2017.03.030

Abdel-Latif IA, Ahmed MR, al-Omari IA, Sellai A (2016) Electrical and magnetic transport in strontium doped europium ferrimanganites. J Magn Magn Mater 420:363–370. https://doi.org/10.1016/j.jmmm.2016.07.016

Abdel-Latif IA (2011) Study on the effect of particle size of strontium - ytterbium manganites on some physical properties. AIP Conf Proc 1370:108–115. https://doi.org/10.1063/1.3638090

Abdel-Latif I A (2020) The particle size effect of $Yb_{0.8}R_{0.2}MnO_3$ (R is Sm, Nd, and Eu) on some physical properties J Nanopart Res 22:45 https://doi.org/10.1007/s11051-020-4759-z

Abdel-Latif I A (2016) Study on structure, electrical and dielectric properties of $Eu_{0.65}Sr_{0.35}Fe_{0.3}Mn_{0.7}O_3$. IOP Conf. Series: Materials Science and Engineering 146: 012003, doi: https://doi.org/10.1088/1757-899X/146/1/012003

Ahmad N., Khan S., Ansari M.M.N., (2018) Microstructural, optical and electrical transport properties of Cd-doped SnO_2 nanoparticles. Mater. Res. Express 5(3): 035045

Ahmed A, Mohamed H, Diab A, Omar E *(2019)* Crossover effect of magnetotransport and magnetocaloric effect in (La0.7Ba0.3MnO3)1-x/(Al2O3)x composites. *Journal of Magnetism and Magnetic Materials 489:* 165388. DOI: https://doi.org/10.1016/j.jmmm.2019.165388

Ayas A O et. al. (2017) Room temperature magnetocaloric effect in $Pr_{1.75}Sr_{1.25}Mn_2O_7$ double-layered perovskite manganite system. Philos. Mag., 10.1080/ 14786435. 2017.1279363

Bashkirov Sh Sh et al. (2003) Crystal structure, electric and magnetic properties of ferrimanganite $NdFe_xMn_{1-x}O_3$. Bulletin of the Russian Academy of Sciences Physics, (Izvestiya Akademii Nauk. Ser. Fizicheskaya) 67: 1165-1169

Bashkirov Sh. Sh. et al. (2005) Mössbauer effect and electrical conductivity studies of $SmFe_xMn_{1-x}O_3$ (x=0.7, 0.8 and 0.9) Journal of Alloys and Compounds 387: 70–73 doi: https://doi.org/10.1016/j.jallcom.2004.06.070

Bettaibi A, et al. (2016) Effect of small quantity of chromium on the electrical, magnetic and magnetocaloric properties of $Pr_{0.7}Ca_{0.3}Mn_{0.98}Cr_{0.02}O_3$ manganite Appl. Phys. A: 122: 232-. https://doi.org/10.1007/s00339-016-9780-9

Bhasin T., et al., (2018) Crystal structure, dielectric, magnetic and magnetoelectric properties of $xNiFe_2O_4$-(1-x)$Na_{0.5}Bi_{0.5}TiO_3$

composites. Journal of Alloys and Compounds 748: 1022-1030 https://doi.org/10.1016/j.jallcom.2018.03.219

Bouziane KA et al (2005) Electronic and magnetic properties of SmFe1-xMnxO3 orthoferrites (x = 0.1, 0.2 and 0.3). *J. Appl. Phys* 97:10A504. https://doi.org/10.1063/1.1851406

Chandran K, Lekshmi PN, Santhosh PN, (2019) High temperature spin reorientation, magnetization reversal and magnetocaloric effect in 50% Mn substituted polycrystalline $ErFeO_3$ Journal of Solid State Chemistry 279: 120910 doi: 10.1016/j.jssc.2019.120910

Cherif R et al (2014) Magnetic and magnetocaloric properties of $La_{0.6}Pr_{0.1}Sr_{0.3}Mn_{1-x}Fe_xO_3$ ($0 \leq x \leq 0.3$) manganites. Journal of Solid State Chemistry 215:271–276. https://doi.org/10.1016/j.jssc.2014.04.004

Dadami ST et al (2017) Impedance spectroscopy studies on PbFe 0.5 Nb 0.5 O 3 –BiFeO 3 multiferroic. Solid Solution Ceramics International 43:16684–16692. https://doi.org/10.1016/j.ceramint.2017.09.059

Dasgupta N et al (2002) Crystal structure and thermal and electrical properties of the perovskite solid solution $Nd_{1-x}Sr_xFeO_3 \pm \delta$ ($0 \leq x \leq 0.4$). Solid State Ionics 149:227–236

Elghoul A, Krichene A, Chniba Boudjada N, Boujelben W (2018) Rare earth effect on structural, magnetic and magnetocaloric properties of $La_{0.75}Ln_{0.05}Sr_{0.2}MnO_3$ manganites. Ceram Int 44(11):12723–12730. https://doi.org/10.1016/j.ceramint.2018.04.075

Hamad M. Kh, et al., (2017) Effect of cobalt doping in $Nd_{1-x}Sr_xMn_{1-y}Co_yO_3$. Journal of Physics: Conf. Series 869: 012032 doi: https://doi.org/10.1088/1742-6596/869/1/012032

Iqbal MJ, Ahmad Z, Meydan T, Melikhov Y (2012) Physical, electrical and magnetic properties of nano-sized Co-Cr substituted magnesium ferrites. J Appl Phys 111:033906. https://doi.org/10.1063/1.3676438

Iqbal M, Khan MN, Khan AA et al. (2017) Structure and charge transport mechanism in hydrothermally synthesized ($La_{0.5}Ba_{0.5}MnO_3$) cubic perovskite manganite J Mater Sci: Mater Electron 28: 15065. 10.1007/s10854-017-7381-9

Kanhere, P. & Chen, Z. A (2014) Review on visible light active perovskite-based photocatalysts. Molecules. 19 (12): 19995–20022; https://doi.org/10.3390/molecules191219995

Kim MK, Moon JY, Oh SH, Oh DG, Choi YJ, Lee N (2019) Strong magnetoelectric coupling in mixed ferrimagnetic-multiferroic phases of a double perovskite. Sci Rep 9:5456. https://doi.org/10.1038/s41598-019-41990-9

Komarov V, Wang S, Tang J (2005) Permittivity and measurements, encyclopedia of RF and microwave engineering, edited by Kai Chang ISBN 0-471-27053-9 *r* : 3693-3711 John Wiley & Sons, Inc.

Kumar Y., et. al., (2016) Effect of heat treatment on the electrical properties of perovskite solar cells, Sol Energy Mater Sol Cells 157: 10–17

Kundu A K., (2016) Magnetic perovskites, Verlag: Springer India, ISBN: 978-81-322-2759-5

Kurbakov A. I. et al., (2019) Study of phase separation phenomena in half-doped manganites with isovalent substitution of rare-earth cations on example of Sm0.32Pr0.18Sr0.5MnO3 Phys. Rev. B 100: 184424

Lee S, Pirogov A, Kang M, Jang KH, Yonemura M, Kamiyama T, Cheong SW, Gozzo F, Shin N, Kimura H, Noda Y, Park JG (2008) Giant magneto-elastic coupling in multiferroic hexagonal manganites. Nature 451:805–809. https://doi.org/10.1038/nature06507

Lee et al (2005) Direct observation of a coupling between spin, lattice, and electric dipole moment in multiferroic YMnO3. Phys Rev B 71:180413R. https://doi.org/10.1103/PhysRevB.71.180413

Mahato Dev K, Saha Sujoy, Sinha TP (2016) Structural studies and impedance spec- troscopy of sol–gel derived $Bi_{0.9}Pr_{0.1}FeO_3$ nanoceramics. J. Physics and Chemistry of Solids;92:45–52

Markovich, V., Puzniak, R., Fita, I. et al. (2013) J Nanopart Res 15: 1862-. 10.1007/s11051-013-1862-4

Naseem S, Khan W, Khan S, Husain S, Ahmad A (2018) Dielectric response and room temperature ferromagnetism in Cr doped anatase TiO_2 nanoparticles J. Magn Magn Mater 447:155–166. https://doi.org/10.1016/j.jmmm.2017.09.051

Parfenov VV et al (2003) Transfer phenomena in $Nd_{0.65}Sr_{0.35}Mn_{1-x}Fe_xO_3$ ferrimanganites. Russ Phys J 46(10):979–980

Parfenov V V et.al., (2007) On the structure and transport mechanism of $Nd_{0,65}Sr_{0,35}Mn_{1-X}Fe_XO_3$ solid solution (X=0, 0.2, 0.4, 0.8). Arab. J. Nucl. Sc. Appl. 40 (1), 167–174

Pattnaik DP, Beardsley RP, Love C, Cavill SA, Edmonds KW, Rushforth AW (2019) Multilevel information storage using magnetoelastic layer stacks. Sci Rep 9:3156. https://doi.org/10.1038/s41598-019-39775-1

Petrov DK, Krusin-Elbaum L, Sun JZ, Feild C, Duncombe PR (1999) Enhanced magnetoresistance in sintered granular manganite/insulator systems. Appl Phys Lett 75(7):995–997

Rajwali K, Fang M.H., (2015) Dielectric and magnetic properties of (Zn, Co) co-doped SnO_2 nanoparticles Chinese Phys. B 24 (12): 127803 10.1088/1674-1056/24/12/127803

Ramesh R, Spaldin N (2007) Multiferroics: progress and prospects in thin films. Nature Mater 6:21–29. https://doi.org/10.1038/nmat1805

Rodriguez-Carvajal (1993) Recent advances in magnetic structure determination by neutron powder diffraction. Physica B.192: 55–69 https://doi.org/10.1016/0921-4526(93)90108-I

Saleh S A et al., (2020) Structural and frequency-dependent dielectric properties of (SnO2)1−x(Fe2O3)x J Nanopart Res 22:44 10.1007/s11051-020-4763-3

Sharma HB, Nomita Devi K, Gupta V, Lee JH, Bobby Singh S (2014) Ac electrical conductivity and magnetic properties of $BiFeO_3$–$CoFe_2O_4$ nanocomposites. J. Alloy Compd 599:32–39. https://doi.org/10.1016/j.jallcom.2014.02.024

Shuk P et al,. *(* 1993) Electrodes for oxygen sensors based on rate earth manganites or cabaltites. Sensors and Actuators *B, 15–16*; 401–405 https://doi.org/10.1016/0925-4005(93)85218-Y

Shuk P and Guth U (1995) Mixed conductive electrode materials for sensors and SOFC Ionics 1: 106. 10.1007/BF02388666

Tokunaga Y, Lottermoser T, Lee Y, Kumai R, Uchida M, Arima T, Tokura Y (2006) Rotation of orbital stripes and the consequent charge-polarized state in bilayer manganites Nat. Mater. 5:973–941. https://doi.org/10.1038/nmat1773

Tugova E, Yastrebov S, Karpov O, Smith R (2017) $NdFeO_3$ nanocrystals under glycine nitrate combustion formation. J Cryst Growth 467:88–92. https://doi.org/10.1016/j.jcrysgro.2017.03.022

Varshney M, Sharma A, Chae KH, Kumar S, Won SO (2018) Electronic structure and dielectric properties of ZrO_2-CeO_2

mixed oxides J. Phys Chem Solids 119:242–250. https://doi.org/10.1016/j.jpcs.2018.04.007

Yousif AA et al (2011) Study on Mossbauer and magnetic properties of strontium doped neodymium ferrimanganites perovskite-like structure. AIP Conf Proc 1370:103–107. https://doi.org/10.1063/1.3638089

Zhang B et al. (2016) Effects of strain relaxation in $Pr_{0.67}Sr_{0.33}MnO_3$ films probed by polarization dependent X-ray absorption near edge structure. *Sci. Rep.* 6: 19886-; doi: https://doi.org/10.1038/srep19886